Asian Journal of Chemistry; Vol. 37, No. 5 (2025), 1134-1140

ASIAN JOURNAL OF CHEMISTRY

https://doi.org/10.14233/ajchem.2025.33321

Development of Reduced Graphene Oxide Ionic Liquid Nanocomposite for the Electrochemical Sensing of Uric Acid

KAVITHA R. THIRUMOORTHI[1], SWAPNA M. GALI[2], S. JAGADESWARAN[1], G.K. JAYAPRAKASH[3] and KIRAN KUMAR TADI[1,*]

[1]Energy, Electrodics and Electrocatalysis (EEE) Research Lab, Department of Chemistry, School of Advanced Sciences, Vellore Institute of Technology, Chennai-600127, India
[2]Department of Physics, Academy of Maritime Education and Training, Chennai-603112, India
[3]Department of Chemistry, Nitte Meenakshi Institute of Technology, Bangalore-560064, India

*Corresponding author: E-mail: kirankumar.tadi@vit.ac.in

Received: 4 January 2025; *Accepted*: 4 April 2025; *Published online*: 30 April 2025; AJC-21980

Graphene-based biosensors are garnering significant scholarly interest attributable to the engineering potential of graphene, which enhances both specificity and sensitivity. However, pristine graphene doesn't account for any specific interactions. The research investigates the utilization of reduced graphene oxide (rGO) in conjunction with hexylmethyl imidazolium tetrafluoroborate ([HMIM]/[BF_4]) ionic liquid (IL) modified glassy carbon electrodes (GCE) for the electrochemical detection of uric acid. Graphene oxide (GO) was synthesized using the improved Hummer's method. Raman spectra was recorded to confirm the exfoliation of graphite to GO and reduction of GO. Cyclic voltammetry and electrochemical impedance spectroscopy were used to study the electron transfer kinetics of the modified electrode. The linearity range of the fabricated sensor was recorded using differential pulse voltammetry (DPV) and observed linearity from 19.6×10^{-6} M to 1.6×10^{-2} M of uric acid concentration with a detection limit of 5.1×10^{-6} M using differential pulse voltammetry (DPV).

Keywords: Uric acid, Electrochemical sensors, Reduced graphene oxide, Ionic liquid.

INTRODUCTION

Uric acid (UA), also known as 2,6,8-trihydroxypurine, is a primary byproduct of biological metabolism. Elevated UA levels in the human body have been associated with various health concerns. Monitoring UA concentrations in body fluids is crucial for identifying the potential diseases and assessing patients with different medical conditions. Disruptions in purine metabolism can lead to UA levels exceeding normal physiological ranges (urine: 2×10^{-3} mol/L, blood: 1.2-4.5 $\times 10^{-4}$ mol/L) [1]. Given the impact of diet and lifestyle on these issues, it is advisable for asymptomatic individuals with elevated UA levels to consider lifestyle changes as a preventive measure. A potential and cost-effective monitoring system is essential to provide accurate feedback and treatment recommendations to hyper uricemic patients.

Conventional approaches for the identification of UA involve the utilization of enzyme-based electrodes alongside high-performance liquid chromatography (HPLC), chemiluminescent methods and an array of spectroscopic techniques [2-6]. HPLC utilizing reversed-phase columns with detection *via* UV absorbance or mass spectrometry was implemented. The traditional methodology for the analysis of UA in clinical laboratories employs the uricase enzyme, which catalyzes the oxidation of UA, resulting in the formation of peroxide, allantoin and carbon dioxide. A different methodology entails the reduction of phosphotungstic acid by uric acid, leading to the production of tungsten blue [7]. Despite the high sensitivity of enzyme based biosensors, they face several challenges. Primarily, the immobilization and stabilization of enzymes are intricate processes. Additionally, enzyme activity is easily affected by various factors such as temperature, pH, humidity and toxic chemicals, leading to poor stability and reproducibility of enzymatic sensors. The high expense of enzymes has intensified the search for enzyme-free sensors as a viable alternative, addressing these challenges.

Furthermore, challenges like poor long-term stability due to surface poisoning from adsorbed intermediate products and interference from coexisting electroactive species persist when

using these electrodes [8]. In addressing these issues and constructing enzyme-free sensors, recent efforts have primarily focused on creating novel sensors with robust electrocatalytic activity and enhanced stability. Due to its simplicity, cost-effectiveness, high sensitivity and selectivity, electrochemical sensors have been used for years to detect many chemical species. Nanostructured materials act as a recognition layer in these sensors, improving mass transfer, surface area, sensitivity, and signal-to-noise ratio. Investigations have been conducted on the use of carbon nanotubes (CNTs) and graphene in conjunction with metals or metal oxides as well as conducting polymers in combination with metals or metal oxides [9]. 2D materials like graphene oxide (GO) and reduced graphene oxide (rGO) are utilized in electrochemical sensing due to their superior electrical conductivity and π-electron transport compared to conventional metal oxides [10].

Graphene, likely composed of sp^2 hybridized carbon atoms arranged in a lattice structure, exhibits exceptional thermal and electrical conductivity, as well as mechanical strength. With a surface area of 2600 $m^2 g^{-1}$, it possesses rapid electron transfer rate [11]. The structural features of graphene significantly contribute to improving both specificity and sensitivity, ranging from small molecules to sensors for high molecular weight proteins [12,13]. It's distinct characteristics, including a large surface area, superior electrical conductivity, and the capacity for surface functionalization, enable it to engage with target molecules in a remarkably precise manner. The surface can be modified to bind only to particular biomolecules, thus improving the specificity of detection. Additionally, the high conductivity enables the detection of even small changes in electrical signals, enhancing sensitivity. This makes it particularly useful in fields like medical diagnostics, environmental monitoring and chemical detection, where precise identification of minute quantities is crucial [14].

Graphene in its pristine form is hydrophobic and resistant to modification. Pristine graphene, while possessing outstanding electrical conductivity and surface area, lacks intrinsic specificity for biomolecular interactions [15]. This limitation affects biosensor performance in several ways such as lack of functional groups (*e.g.* carboxyl, hydroxyl, or amine) that are necessary for covalent attachment of biomolecules like antibodies, aptamers, or enzymes. Due to strong π-π interactions of pristine graphene can adsorb various biomolecules non-selectively, leading to high background signals, false positives, reduced sensitivity due to unwanted interactions [16]. However, GO produced by oxidizing graphite, introduces oxygen functional groups, making it highly dispersible in solutions [17]. Upon reduction of rGO through chemical or thermal processes, the removal of substantial oxygen functional groups results in the formation of rGO. Despite the reduction, the remaining oxygen functional groups facilitate effective dispersion and chemical modification of rGO [18]. The restoration of carbon-conjugated networks during reduction leads to improved conductivity in rGO compared to graphene. Due to these distinctive properties, both GO and rGO are considered to make significant contributions to electrochemical sensing applications, surpassing conventional metals and metal oxides.

Given that UA can be readily oxidized in aqueous solutions using traditional electrodes to yield allantoin as the primary product, non-enzymatic electrochemical approaches have emerged as viable alternatives. Biological fluids like blood and urine contain UA and ascorbic acid (AA). However, the oxidation of UA at metal electrodes requires substantial overpotentials and the oxidation potentials of UA and AA are closely situated, leading to poor selectivity at standard electrodes [19]. Establishing a selective method for UA determination is crucial for accurate and specific electroanalytical research. Since the baseline concentration of UA in physiological samples varies depending on the matrix, both sensitivity and selectivity are pivotal in the development of electrochemical assays.

Electrodes modified with rGO for the selective detection of UA offer several advantages in electroanalysis. These modifications, particularly those involving rGO, help overcome issues such as saturation of active binding sites, which can limit the linear range of non modified electrodes. The incorporation of rGO with glassy carbon electrodes (GCE) enhances sensitivity, lowers detection limits and increases the efficiency of electron transfer, making it a focal point in the study. This research aims to comprehensively explore the electrochemical sensing of UA using cyclic voltammetry, emphasizing the use of modified electrodes in the detection process.

Ionic liquids (ILs) play a significant role in the realm of green chemistry due to their distinctive characteristics and garnered for a variety of applications [20]. Numerous studies in biosensors have focused on the utilization of different ILs either as a supportive medium or as an electrode modifier. The stability, selectivity and sensitivity of the electrodes are increased when ILs are used as sensing materials. ILs in conjunction with carbon nanomaterials, particularly graphene, enhances electrocatalytic activity as well as the efficacy of heterogeneous electron transfer [21].

In present work, a simple strategy for the sensing of UA using IL, hexylmethylimidizolium tetrafluorborate (HMIM/BF_4) embedded rGO on a glassy carbon electrode is developed. The IL (HMIM/BF_4) was synthesized according to our previous report [22]. The sensor shows excellent electrocatalytic activity towards UA and the corresponding diffusion-controlled reaction was studied using CV. Moreover, the linearity and the detection limit of sensor towards UA was tested using differential pulse voltammetry (DPV). The fabricated electrode shows excellent reproducibility, repeatability and long-term stability without any fouling characteristics.

EXPERIMENTAL

All chemicals and materials were used as obtained from the commercial vendors unless it is mentioned. Graphite SRL 98.5% (purity), sulphuric acid (H_2SO_4) 98%, phosphoric acid (H_3PO_4), potassium permanganate ($KMnO_4$), hydrochloric acid (HCl), ethanol (C_2H_6O) and uric acid (UA, $C_5H_4N_4O_3$) were purchased from Sigma-Aldrich, USA. Sodium hydroxide (NaOH), potassium ferricyanide ($K_3[Fe(CN)_6]$, potassium ferrocyanide ($K_4[Fe(CN)_6]$), potassium chloride (KCl), potassium dihydrogen phosphate (KH_2PO_4), dipotassium hydrogen phosphate (K_2HPO_4)

and alumina powder (50 nm) were procured from SRL Chemicals, Mumbai, India. All aqueous solutions were prepared in purified Millipore water obtained using the Milli-Q system (Millipore Inc.).

All electrochemical measurements including cyclic voltammetry (CV), chronoamperometry (CA) and electrochemical impedance spectroscopy (EIS) were conducted by a typical three-electrode electrochemical cell controlled by Palmsens potentiostat (Model: EmStatHR) interfaced with PStrace software. Glassy carbon electrodes (GCE) of 3 mm, platinum wire and Ag/AgCl (3 M KCl) were used as the working electrolyte, counter electrode and reference electrode respectively. Electrochemical impedance spectroscopy was conducted in a Fe redox probe $[Fe(CN)_6]^{-3/-4}$ over a frequency range of 100,000 to 0.01 kHz at an AC voltage of 10 mV and a DC voltage of 0.22V applied with respect to the reference electrode Ag/AgCl (3 M KCl).

Raman spectra were recorded on a laser confocal Raman micro spectrometer (HR-800, Horiba Jobin Yvon, Ltd.), with an excitation laser wavelength of 532 nm. JEOL Japan Make, JSM 7200F (model) was used to capture FESEM images.

Synthesis of rGO: GO was prepared *via* improved synthesis of GO as reported in the literature [23]. According to the procedure, bulk graphite flakes were treated with conc. H_2SO_4 and H_3PO_4 (9:1 v/v, 360 mL: 40 mL). This was followed by pinch-by-pinch addition $KMnO_4$ (18 g, 6 wt. equiv.). The reactants were heated to 90 ºC and agitated for 12 h and consequently cooled to 27 ºC. Prior to this, the reaction vessel was placed in an ice bath and 3 mL of 30% H_2O_2 was added and agitated for 2 h. The following suspension was rinsed thoroughly with water, 30 % HCl and ethanol, washing the precipitate till the pH of the solution was impartially dry. The precipitation was dried in a hot air oven for 1 h at 60 ºC. Then, as-synthesized GO (90 mg) was heated in a laboratory warm air oven at 90 ºC for 3 h. As a result oxides were removed [24] and the ensuing decreased GO is 83 mg.

Synthesis of HMIM/BF_4 (IL): The HMIM/BF_4 (IL) was prepared as per reported literature [22]. In brief, hexyiodide and 1-methylimidazole (1/1.5 v/v ratio) were stirred thoroughly for 50 h for 700 rpm at 30 ºC. This was followed by washing the reaction mixture with ethyl acetate to remove the unreacted precursors. The resultant product was treated with 23 g of $NaBF_4$ and stirred for 48 h at 60 ºC. The reaction mixture was purified using the activated charcoal at 70 ºC and followed by fractional distillation to separate based on their boiling points. Finally, the reaction mixture was taken in a 50 mL round bottom flask and rota-evaporated gradually for the final purification.

Fabrication of sensor: Homogeneous dispersion of rGO was mixed with IL (1:1 v/v) and sonicated for 1 h. GCE (3 mm in dia) was well polished on polishing paper with 50 nm alumina particles containing slurries. The electrodes were ultrasonicated in ethanol and water and then washed exhaustively with ultrapure water to acquire a fresh and clean surface and dried in air. The GCE was fabricated by drop-casting of 5 µL as-synthesized rGO/IL on the mirror-finished GCE and dried under ambient conditions. The modified electrode GCE/rGO/IL was used for the sensing of UA by CV and DPV techniques.

RESULTS AND DISCUSSION

The Raman spectra of graphite, GO and rGO were examined using a micro-Raman spectrometer, revealing two major peaks: the G-band and D-band (Fig. 1). The D-band, observed at 1359 cm^{-1}, signifies structural defects arising from coupled hydroxyl and epoxide groups in the carbon-based material. The G-band at 1614 cm^{-1}, generated through E_{2g} mode first order scattering, experiences a shift to a higher frequency in graphene oxide due to a reduced number of second sheets and the formation of isolated double bonds disconnected from functional groups within the carbon network [25]. This shift distinguishes the G-band frequency in graphene oxide from that in graphite.

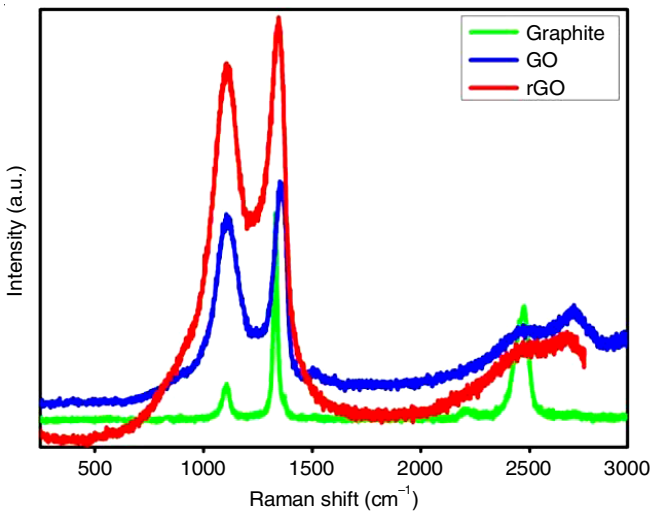

Fig. 1. Raman spectra of rGO, GO and graphite

The D/G band intensity ratio serves as a parameter linked to an increase in contamination concentration, with higher contamination leading to a raised D/G ratio. Electrochemical reduction of graphene oxide (ERGO) reduces sp^2 domains, contributing to an elevated D/G ratio in ERGO. The reduction in the typical extensive sp^2 domains within the graphene lattice results in the comparatively high D/G ratio of RGO (0.91) compared to graphene (0.85) and graphite (0.18). To summarize, the analysis of Raman spectra unveils distinctive features in the G-band and D-band peaks, offering insights into structural defects, changes in carbon bonding and contamination levels in graphene-based materials. The D/G ratio emerges as a valuable indicator, reflecting alterations induced by electrochemical processes and variations in the graphene lattice structure [26].

Morphological studies: SEM images of GO (Fig. 2) revealed two-dimensional nanosheet structures characterized by wrinkled and folded textures. These sheets often exhibit irregular edges, rough surfaces and crumpled areas due to scrolling effects. Observations using SEM have shown GO sheets with lateral sizes reaching up to 200 µm, alongside fragments as small as a few microns within the same sample.

Electrochemical characterization: The modification GCE involved cyclic voltammetry (CV) at various modifications within the potential range of -0.3 V to +0.6 V, utilizing a scan rate of 100 mV/s. The redox probe $[Fe(CN)_6]^{-3/-4}$, along with 0.1

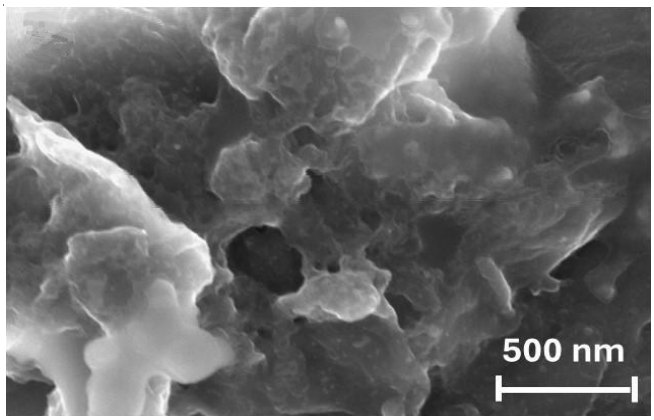

Fig. 2. SEM image of GO

M KCl was employed as a supporting electrolyte. In the absence of any modification, the bare glassy carbon electrode (GCE) displayed a low redox peak current (~0.75 mA) with sluggish electron transfer kinetics revealed from broad potential difference (Fig. 3a). With the modification of GO, there was a noticeable decrease in the redox peak currents (0.65 mA) due to the presence of negative carboxyl functional groups which decreases the conductivity of graphite. However, further modifications with rGO and rGO-IL resulted in the significant enhancement in the redox peak current (1.2 mA) and decrease in the peak potential difference to 80 mV. This reduction in ΔE is attributed to the improved electron transfer kinetics facilitated by the introduction of the IL, enhancing the electrode's performance.

The modified GCE/rGO-IL surface was carried out using electrochemical impedance spectroscopy (EIS), a highly sensitive technique for studying interface properties of functionalized surfaces [27]. Nyquist plots in Fig. 3b illustrate the impedance characteristics of the modified electrodes. The Nyquist plots analysis revealed that the modified GCE/rGO-IL surface exhibited the lowest charge transfer resistance (R_{CT}). This observation further supports the enhanced electron transfer kinetics achieved through the synergistic effect of rGO-IL modification (RCT – 158 Ω). In contrast, GO and rGO modified surfaces exhibited 196 higher R_{CT} values *ca.* 1450 Ω and 855 Ω, respectively. The combined analyses of CV and EIS provide a comprehensive understanding of the electrochemical performance of the modified electrode, emphasizing the significance of IL in optimizing electron transfer dynamics.

Electrochemical sensing of UA: Cyclic voltammetry (CV) serves as a commonly applied electrochemical method for investigating the redox properties of diverse substances. In this study, CV is conducted using different modified electrodes in a phosphate buffer with a pH of 7.2 (0.1 M), including GO, rGO and rGO-IL (Fig. 4a).

As is observed from Fig. 4a, the electrode GO/GCE shows relatively insignificant anodic peak current (0.1 mA) for UA at potential (0.41 V) and shows irreversible behavior. However, after the reduction of GO, there is a noticeable increase in the peak current (0.2 mA). The highest peak current (0.40 mA) is observed for the rGO with ionic liquid (rGO-IL) modified GCE, which is significantly higher than that of rGO/GCE. This enhancement in the peak current suggests an improvement in the sensitivity of sensitive, which may also contribute to a lower limit of detection for UA. This is attributed to enhancement in the conductivity of rGO-IL composite, upon embedding of $HMIM/BF_4$ ionic liquid in the sp^2 conjugated bonds in lattice of rGO. The aim is to detect UA and the noteworthy observation is that reduced graphene demonstrates a significant current at an anodic peak potential of 0.5 V.

The electrochemical responses of UA in a 0.1 M phosphate buffer solution were examined on a rGO ionic liquid-modified glassy carbon electrode (rGO-IL/GCE) using cyclic voltammetry (CV) with varying scan rates from 10 mV/s to 100 mV/s, as depicted in Fig. 4b.

As the scan rate increased, there was a corresponding rise in peak currents. The relationship between the square root of the scan rate and the corresponding peak current as observed in the linear correlation presented in Fig. 5a, aligns with the Randles-Sevcik equation [28]. This finding suggests a diffusion controlled oxidation reaction of UA at the GCE/rGO-IL interface. The relationship is expressed by eqn. 1:

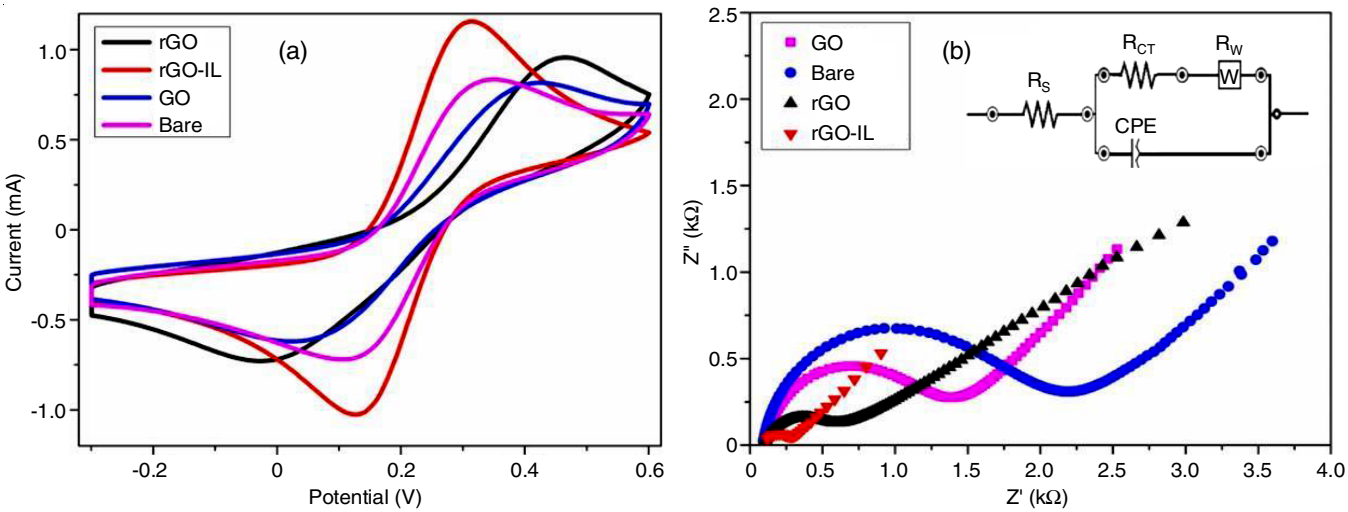

Fig. 3. (a) CVs and (b) Nyquist plots of the modified GCE at different stage of GO, rGO, rGO-IL modified and unmodified GCE recorded in the redox probe 5 mM $[Fe(CN)_6]^{-3/-4}$ containing 0.1 M KCl

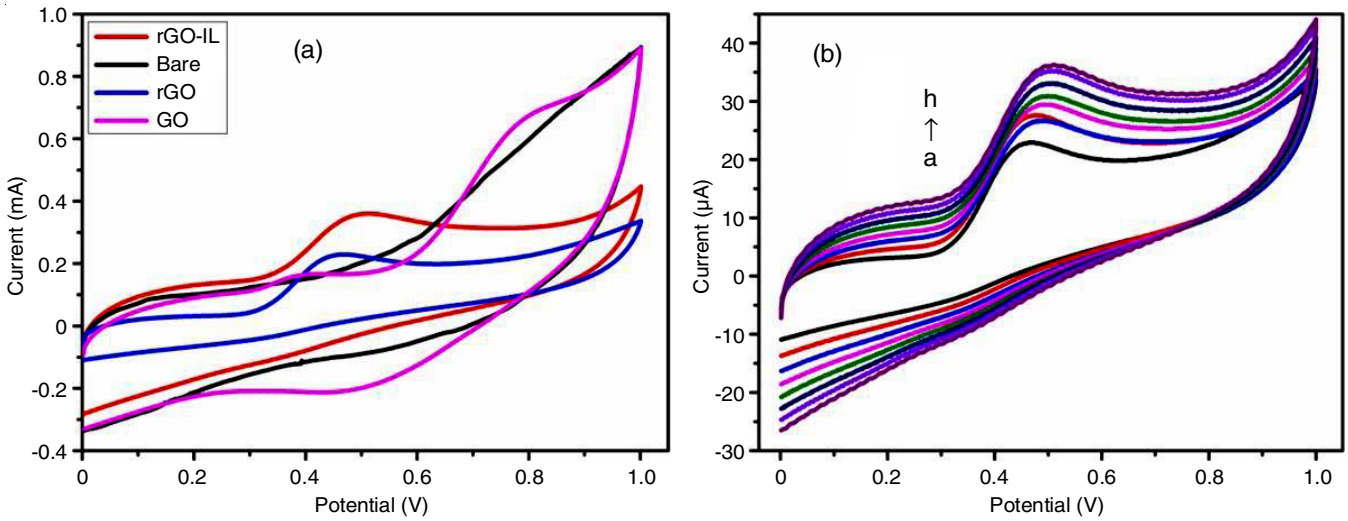

Fig. 4. (a) CVs of GO, rGO, rGO-IL modified GCEs and bare GCE conducted in 100 μM UA and (b) CVs rGO-IL modified GCE in 100 μM UA at various scan rates starting from 10 to 100 mV/s

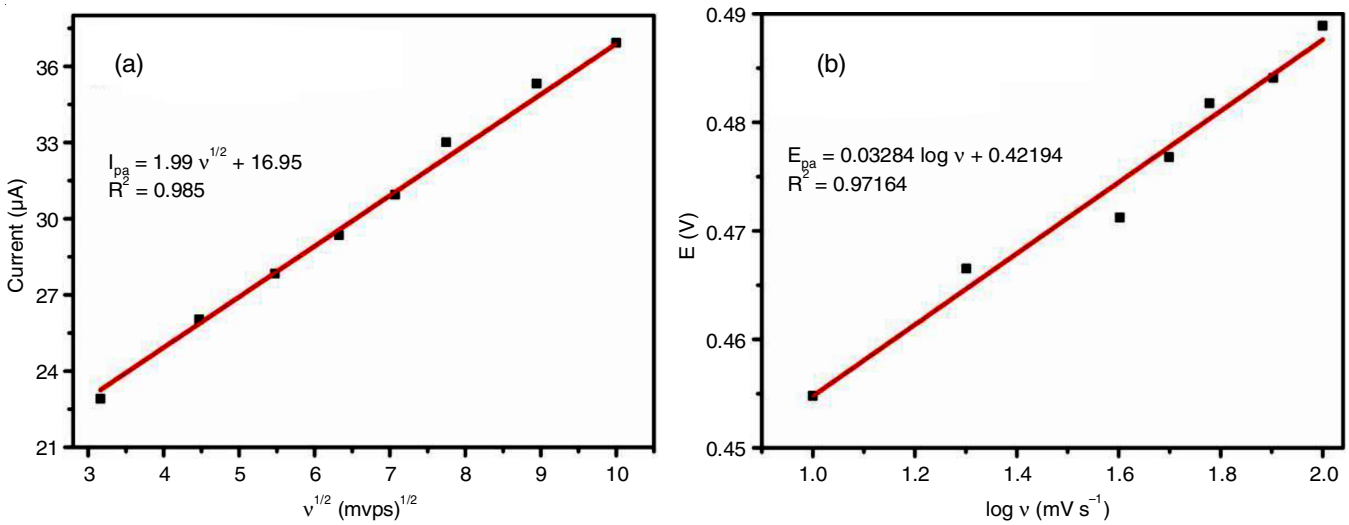

Fig. 5. (a) Linear plot between square root of scan rate and anodic peak current and (b) Tafel's plot showing the change in anodic peak potential (E_{pa}) *vs.* logarithm of scan rate (log ν)

$$I_p = 0.227\ FAC_0k_0 \exp\left[-\alpha f(E_p - E_0)\right] \quad (1)$$

Theses investigation indicates that the electrochemical behavior of UA at the GCE/rGO-IL electrode is consistent with a diffusion-controlled reduction reaction, as evidenced by the observed trends in cyclic voltammetry.

To understand the mechanism of number of electrons involved in the electrochemical oxidation of UA at the rGO-IL/GCE, change in the anodic peak potential (E_{pa}) with respect to logarithm of scan rate was plotted (Fig. 5b) according to Tafel's equation (eqn. 2).

$$E_p = \frac{b}{2}\log \nu + \text{Constant} \quad (2)$$

where E_p refers to anodic peak potential; ν is the scan rate; and b is the Tafel's slope. Eqn. 2 is valid for an irreversible diffusion controlled reaction. However,

$$b = \frac{2.303RT}{nF(1-\alpha)} \quad (3)$$

where n is the number of electrons involved in the reaction; α is the electron transfer coefficient; and F is Faraday constant (96,500 C/mol). From Fig. 5b, Tafel's slope (b) was calculated to be 0.064 V. On assuming α value for the irreversible reaction as 0.50 and substituting the b value in eqn. 3; the number of electrons (n) value was obtained as 1.87 (~2) confirming the mechanism of UA oxidation as reported in the literature [29].

Dose response of UA using rGO-IL/GCE: DPV has been adopted to study the dose response of UA to rGO-IL/GCE due of its higher current sensitivity and better resolution than CV. In this regard, the concentration of UA additions of UA were successively increased and recorded the corresponding DPV on each addition. As can be observed from Fig. 6a, two anodic peaks at potentials (0.6 V and 0.7 V) increased in the addition to UA ranging from 19.6×10^{-6} M to 1.6×10^{-2} M. The oxidation of UA is well-known and proceeds through formation of unstable diamine involving two electron transfer. Electrochemcial oxidation of UA to UA anion (I), leading to

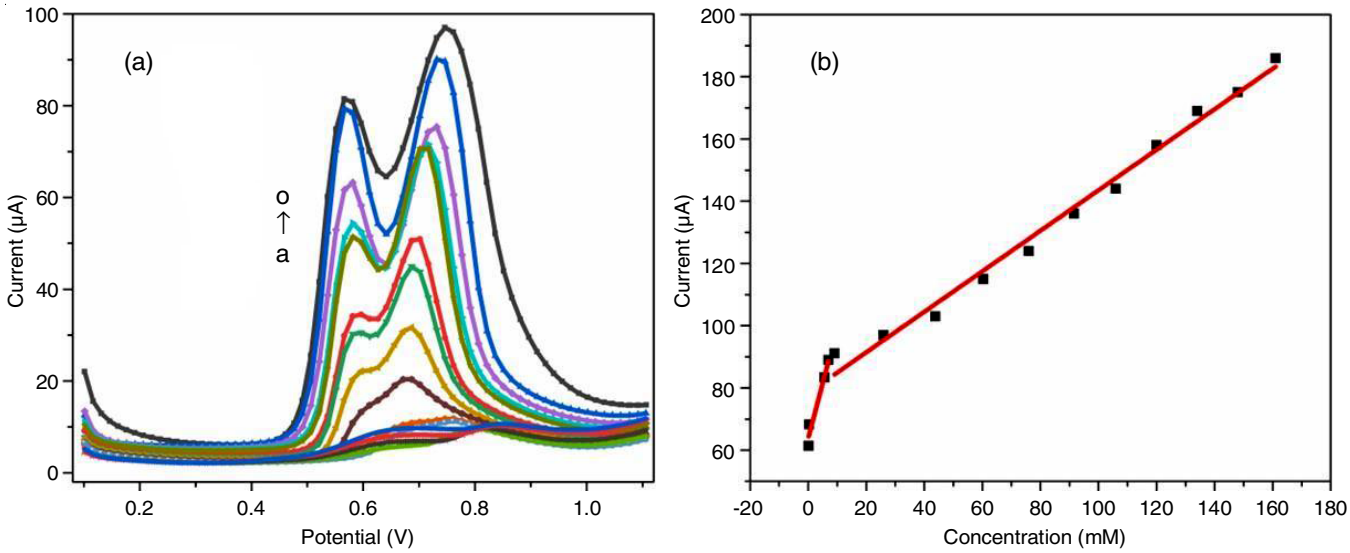

Fig. 6. (a) Overlay of DPVs obtained at rGO-IL/GCE in 0.1 M phosphate buffer solution (pH 7.2) containing various concentrations of UA from 19.6×10^{-6} M to 1.0×10^{-2} M and (b) corresponding calibration curves of UA obtained from the anodic peak currents of DPVs with respect to UA concentration

the formation of an unstable anionic quinoid, which further yields allantoin as product.

On fitting the anodic peak current at 0.6 V with the concentration of UA (Fig. 6b), two linear regions were found with the linear regression equations:

$$I\ (\mu A) = 0.00355[UA]\ \mu M + 6.3731 \times 10^{-5}\ (R^2 = 0.9403)\ (4)$$

$$I\ (\mu A) = 0.00651[UA]\ \mu M + 7.84208 \times 10^{-5}\ (R^2 = 0.9874\ (5)$$

The former linearity corresponding to UA concentration from 19.6×10^{-6} M to 9.09×10^{-3} M, while the later corresponding to 2.6×10^{-3} M to 1.61×10^{-2} M and the limit of detection (LOD) was found to be 5.10×10^{-6} M. LOD of the sensor was determined using the relation between slope of the calibration curve (s) and the standard deviation of blank (σ) and as follows LOD = 3 s/σ. The linearity ranges and LOD of the recently reported materials for the electrochemical detection of UA are compared with the present work (Table-1).

Conclusion

Ionic liquid (IL) modified reduced graphene oxide (rGO) showed excellent electrocatalytical properties to uric acid (UA) oxidation. Utilizing rGO-IL in conjunction with GCE enabled the execution of DPV and CV to assess the electron transfer behaviour of UA. There is a significant improvement in the electron transfer after modification of GCE with IL/rGO as observed from the CV and EIS. The electrochemical signal for UA was doubled using IL/rGO compared to rGO. Compared to rGO, IL/rGO The detection limit (LOD) for UA was expressed in micromolar units. Further, the fabricated sensor showed a wide linear range and low detection limit for the determination of UA. The findings indicate that rGO-IL exhibits favourable electron transport characteristics, making it a promising material for the precise determination of UA. The work summarizes the beneficial electron transport properties of rGO-IL are particularly advantageous for the determination of UA due to their ability to facilitate efficient electron flow during the electrocatalytic reaction. The combination of the ultra-low thickness layered nanomaterial and IL, enhances the sensitivity and accuracy of UA detection, which is essential for reliable biosensor performance. In real-world applications, such as in medical diagnostics or wearable health-monitoring devices, these properties enable the development of sensors that are both quick and highly responsive, making them valuable for continuous monitoring of UA levels, especially for conditions like gout or kidney disease. Additionally, the stability and versatility of rGO-IL-based materials offer potential for scalable biosensor production. Future research could focus on further optimizing the selectivity of these sensors, possibly by exploring the integ-

TABLE-1
COMPARISON OF LINEAR RANGE AND DETECTION LIMITS WITH THE SENSORS REPORTED FOR URIC ACID

S. No.	Electrode material	Electrochemical technique	Linearity range (μM)	LOD (μM)	Ref.
1	HADC-IL	DPV	2-1050	1.27	[29]
2	Cu-BTC MOF	DPV& CA	0.5-600.0	0.20	[30]
3	HAP	DPV	0.068-50.0	0.05	[31]
4	N-rGO	DPV	1-30	0.20	[32]
5	rGO-AuNPs	LSV	10-500	3.60	[33]
6	Ru-Ala-C_3N_4	CA	595-2135	0.17	[34]
7	ZnO NRs-CuO NS	DPV	2-2000	0.28	[35]
8	$NiMn_2O_4$/GP		3-120	0.40	[36]
9	rGO/HMIM	DPV	19.6-16100	5.10	Present work

ration of other nanomaterials or fine-tuning the ionic liquid composition to improve long-term performance as well as enhance detection limits.

ACKNOWLEDGEMENTS

One of the authors, Kavitha Rani thanked Vellore Institute of Technology, Chennai, India for providing the PhD fellowship. The authors thank School of Advanced Sciences, VIT, Chennai, India for facilitating infrastructure and characterization to conduct the research work.

CONFLICT OF INTEREST

The authors declare that there is no conflict of interests regarding the publication of this article.

REFERENCES

1. J. Maiuolo, F. Oppedisano, S. Gratteri, C. Muscoli and V. Mollace, *Int. J. Cardiol.*, **213**, 8 (2016); https://doi.org/10.1016/j.ijcard.2015.08.109
2. D. Swinson, J. Snaith, J. Buckberry and M. Brickley, *Int. J. Osteoarchaeol.*, **20**, 135 (2010); https://doi.org/10.1002/oa.1009
3. N. Duplancic, D. Kukoc-Modun, L. Modun and D. Radic, *Molecules*, **16**, 7058 (2011); https://doi.org/10.3390/molecules16087058
4. F.R.P. Rocha and D.L. Rocha, *Microchem. J.*, **94**, 53 (2010); https://doi.org/10.1016/j.microc.2009.08.010
5. M.L. Jin, D. Seo, M.H. Huy, B.T. Pham, Q.T. Conte, Y.-I. Thangadurai and D. Lee, *Biosens. Bioelectron.*, **77**, 359 (2016); https://doi.org/10.1016/j.bios.2015.09.057
6. Z. Zhang, Y. Jin, X. Li, J. Zhao, X. Guo, J. Wang, Z. Guo, X. Zhang, Y. Tao, Y. Liu, D. Chen and X. Liang, *J. Chromatogr. B Analyt. Technol. Biomed. Life Sci.*, **1026**, 67 (2016); https://doi.org/10.1016/j.jchromb.2015.11.015
7. M.B. Blauch and F.C. Koch, *J. Biol. Chem.*, **130**, 443 (1939); https://doi.org/10.1016/S0021-9258(18)73516-3
8. G. Li, C. Xu, H. Xu, L. Gan, K. Sun and B. Yuan, *Analyst*, **148**, 2553 (2023); https://doi.org/10.1039/D3AN00291H
9. Geethukrishnan, O. Apte and K.K. Tadi, *Tungsten*, **7**, 137 (2024); https://doi.org/10.1007/s42864-024-00297-7
10. C. Wang, P. Xu and K. Zhuo, *Anal. Sci.*, **26**, 191 (2014); https://doi.org/10.1002/elan.201300345
11. M. Pumera, *Chem. Rec.*, **9**, 211 (2009); https://doi.org/10.1002/tcr.200900008
12. D. Li, J. Liu, C.J. Barrow and W. Yang, *Chem. Commun.*, **50**, 8197 (2014); https://doi.org/10.1039/c4cc03384a
13. S. Xu, T. Wang, G. Liu, Z. Cao, L.A. Frank, S. Jiang, C. Zhang, Z. Li, V.V. Krasitskaya, Q. Li, Y. Sha, X. Zhang, H. Liu and J. Wang, *Sens. Actuators B Chem.*, **326**, 128991 (2021); https://doi.org/10.1016/j.snb.2020.128991
14. A.R. Jalalvand and M.M. Karami, *Sens. Bio-Sens. Res.*, **47**, 100733 (2025); https://doi.org/10.1016/j.sbsr.2024.100733
15. N. Mushahary, A. Sarkar, F. Basumatary, S. Brahma, B. Das and S. Basumatary, *Result Surfaces Interfaces*, **15**, 10025 (2024); https://doi.org/10.1016/j.rsurfi.2024.100225
16. S.S. Sekhon, P. Kaur, Y.H. Kim and S.S. Sekhon, *npj 2D Mater. Appl.*, **5**, 21 (2021); https://doi.org/10.1038/s41699-021-00202-7
17. J. Liu, C. Shuping, L. Yanan and Z. Bijing, *J. Saudi Chem. Soc.*, **26**, 101560 (2022); https://doi.org/10.1016/j.jscs.2022.101560
18. P.L. Yap, S. Kabiri, Y.L. Auyoong, D.N.H. Tran and D. Losic, *ACS Omega*, **4**, 19505 (2019); https://doi.org/10.1021/acsomega.9b02642
19. P. Klemp, S.A. Stansfield, B. Castle and M.C. Robertson, *Ann. Rheum. Dis.*, **56**, 22 (1997); https://doi.org/10.1136/ard.56.1.22
20. D. Isin, E. Eksin and A. Erdem, *Biosensors*, **12**, 95 (2022); https://doi.org/10.3390/bios12020095
21. K. Chen, B. Xu, L. Shen, D. Shen, M. Li and L.-H. Guo, *RSC Adv.*, **12**, 19452 (2022); https://doi.org/10.1039/D2RA02547G
22. P. Kumar, I. Soni, G.K. Jayaprakash, S. Kumar, S. Rao, R. Flores-Moreno and A.S. Sowmyashree, *Inorg. Chem. Commun.*, **146**, 110110 (2022); https://doi.org/10.1016/j.inoche.2022.110110
23. D.C. Marcano, D.V. Kosynkin, J.M. Berlin, A. Sinitskii, A. Slesarev, Z. Sun, L.B. Alemany, W. Lu and J.M. Tour, *ACS Nano*, **4**, 4806 (2010); https://doi.org/10.1021/nn1006368
24. N. Murugesan, M. Kandasamy, S. Murugesan, N. Pugazhenthiran, S. Suresh, V.P. Venkatesh, B.K. Balachandar, S.K. Kumar and M.N.M. Ansari, *Physica B*, **669**, 415288 (2023); https://doi.org/10.1016/j.physb.2023.415288
25. A.C. Ferrari and D.M. Basko, *Nat. Nanotechnol.*, **8**, 235 (2013); https://doi.org/10.1038/nnano.2013.46
26. S.I. Khan, K.K. Tadi, R.R. Chillawar and R.V. Motghare, *J. Electrochem. Soc.*, **165**, B804 (2018); https://doi.org/10.1149/2.0121816jes
27. J.G. Gu, S.P. Cheng, J. Liu and J.D. Gu, *J. Polym. Environ.*, **8**, 167 (2000); https://doi.org/10.1023/A:1015293626335
28. A.J. Bard and L.R. Faulkner, Electrochemical Sensors: Fundamental and Applications, John Wiley & Sons, Inc. edn. 2 (2001).
29. Y. Abbas, S. Ali, M. Basharat, W. Zou, F. Yang, W. Liu, S. Zhang, Z. Wu, N. Akhtar and D. Wu, *ACS Appl. Nano Mater.*, **3**, 11383 (2020); https://doi.org/10.1021/acsanm.0c02466
30. A. Ajith, N.S.K. Gowthaman, D. Pandiarajan, C. Sugumar and S.A. John, *Microchem. J.*, **199**, 110020 (2024); https://doi.org/10.1016/j.microc.2024.110020
31. E. Iyyappan, S.J. Samuel Justin, P. Wilson and A. Palaniappan, *ACS Appl. Nano Mater.*, **3**, 7761 (2020); https://doi.org/10.1021/acsanm.0c01322
32. H. Zhang and S. Liu, *J. Alloys Compd.*, **842**, 155873 (2020); https://doi.org/10.1016/j.jallcom.2020.155873
33. F. Mazzara, B. Patella, G. Aiello, A. O'Riordan, C. Torino, A. Vilasi and R. Inguanta, *Electrochim. Acta*, **388**, 138652 (2021); https://doi.org/10.1016/j.electacta.2021.138652
34. X. Xie, D.P. Wang, C. Guo, Y. Liu, Q. Rao, F. Lou, Q. Li, Y. Dong, Q. Li, H.B. Yang and F.X. Hu, *Anal. Chem.*, **93**, 4916 (2021); https://doi.org/10.1021/acs.analchem.0c05191
35. S. Masrat, V. Nagal, M. Khan, A. Ahmad, M.B. Alshammari, S. Alam, U.T. Nakate, B. Lee, P. Mishra, K.S. Bhat and R. Ahmad, *ACS Appl. Nano Mater.*, **6**, 16615 (2023); https://doi.org/10.1021/acsanm.3c02794
36. S. Pramanik, P. Karmakar and D.K. Das, *Biointerface Res. Appl. Chem.*, **13**, 134 (2022); https://doi.org/10.33263/BRIAC132.134